METALLOPROTEINS

A complex iron-calcium cofactor catalyzing phosphotransfer chemistry

Shee Chien Yong,[1]* Pietro Roversi,[2]*† James Lillington,[2]‡ Fernanda Rodriguez,[1] Martin Krehenbrink,[1]§ Oliver B. Zeldin,[1]|| Elspeth F. Garman,[1] Susan M. Lea,[2]¶ Ben C. Berks[1]¶

Alkaline phosphatases play a crucial role in phosphate acquisition by microorganisms. To expand our understanding of catalysis by this class of enzymes, we have determined the structure of the widely occurring microbial alkaline phosphatase PhoX. The enzyme contains a complex active-site cofactor comprising two antiferromagnetically coupled ferric iron ions (Fe^{3+}), three calcium ions (Ca^{2+}), and an oxo group bridging three of the metal ions. Notably, the main part of the cofactor resembles synthetic oxide-centered triangular metal complexes. Structures of PhoX-ligand complexes reveal how the active-site metal ions bind substrate and implicate the cofactor oxo group in the catalytic mechanism. The presence of iron in PhoX raises the possibility that iron bioavailability limits microbial phosphate acquisition.

P hosphate-containing macromolecules and metabolites are essential components of living cells. Under conditions of phosphate deficiency, microorganisms obtain phosphate from biologically derived organic compounds by producing extracytoplasmic alkaline phosphatases (1, 2). Prominent among these enzymes are phosphate monoesterases of the PhoA and PhoX families, which are found in all three domains of life. The archetypal PhoA enzyme of *Escherichia coli* has been extensively studied (2), but PhoX alkaline phosphatases are minimally characterized and do not exhibit sequence similarity to other phosphotransfer enzymes. Genes encoding PhoX are abundant in ocean bacteria (3–5) and are also present in bloom-forming cyanobacteria (6), human pathogens (7, 8), and eukaryotic green algae, including the model organism *Chlamydomonas reinhardtii* (9).

To establish the active-site architecture of PhoX, we have undertaken structural analysis of the enzyme from *Pseudomonas fluorescens* Pf0-1 (10). Recombinant *P. fluorescens* PhoX is a phosphomonoesterase with no phosphodiesterase activity and is able to cleave phosphorus-nitrogen bonds but not phosphorus-carbon bonds (fig. S1A). The purified PhoX protein is purple in color with several broad absorbance bands in the visible spectrum, indicating the presence of a prosthetic group (Fig. 1A). Addition of adenosine-5′-(β,γ-methylene)triphosphate (AMP-

PCP), a nonhydrolyzable analog of the substrate ATP, causes changes in the visible spectrum (Fig. 1A), showing that the prosthetic group is associated with the substrate-binding site. We determined crystal structures for native PhoX and for PhoX in complex with AMP-PCP, phosphate, and the putative transition-state mimic vanadate. All four structures were determined to high resolution (1.1 to 1.5 Å) from crystals grown at the catalytic pH optimum of 8 (figs. S1B, S2A, and S3, and tables S1 and S2).

PhoX folds as a six-bladed β propeller (Fig. 2A). The active site of the enzyme lies at the bottom of the cavity at the center of the propeller and is accessible from only one face of the propeller

through a channel (Fig. 2B). The active site in the native PhoX structure contains four metal ions, and a further metal ion is present in the structures of the three PhoX-ligand complexes. Proton-induced x-ray emission spectroscopy of a sample of the PhoX-phosphate complex detected 3.4 ± 0.3 atoms of calcium and 1.6 ± 0.1 atoms of iron per complex, with no other candidate elements (Co, Ni, Zn, Mg, and Mn) detectable. Individual metal ion sites in the PhoX structures were assigned as three Ca and two Fe ions on the basis of their coordination geometry and anomalous scattering at different wavelengths (fig. S2, B and C). All metal sites are fully occupied, and the B factors are similar for the Ca and Fe ions. The ions Fe_A, Fe_B, and Ca_A form a triangle at the bottom of the active-site cavity (Figs. 2 and 3). Ions Ca_B and (in the ligand complexes only) Ca_C lie above the plane of the first three ions and to one side of the cavity, with the plane containing the three Ca ions being almost perpendicular to that of the $Fe_A Fe_B Ca_A$ triangle. All five metal ions are coordinated by oxygen atoms provided either by the side chains of conserved residues, by water, or by the ligand molecules (Fig. 2C and figs. S3 and S4, A, D, and E, and table S3). Fe_A is additionally ligated by a thiolate side chain from invariant Cys^{179}. Substitution of individual amino acids coordinating Fe_A, Fe_B, Ca_B, or Ca_C resulted in PhoX variants with either no, or trace, catalytic activity (table S4).

Electron paramagnetic resonance (EPR) spectroscopy was used to determine the oxidation state of the PhoX iron atoms (Fig. 1B). The native PhoX protein was EPR-silent. However, partial reduction of the protein with dithionite led to the appearance of an EPR signal at an effective g value of 4.3 characteristic of monomeric
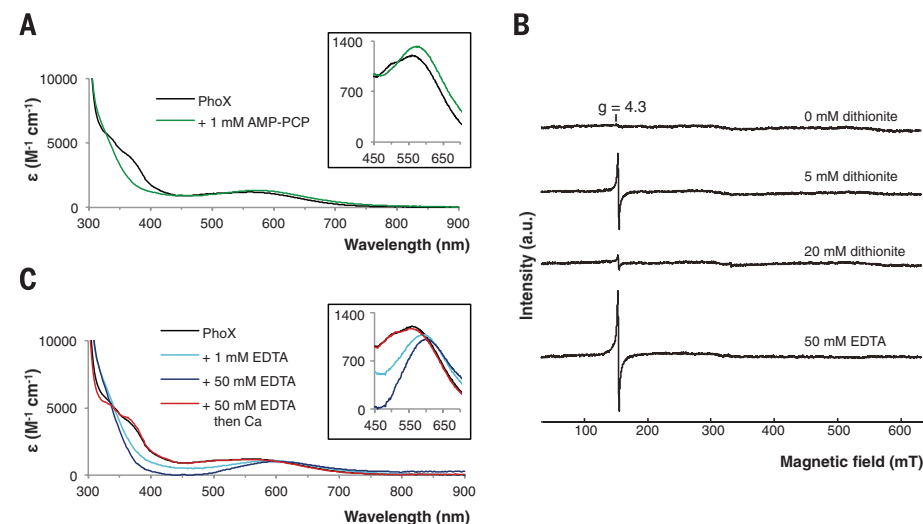
[1]Department of Biochemistry, University of Oxford, South Parks Road, Oxford OX1 3QU, UK. [2]Sir William Dunn School of Pathology, University of Oxford, South Parks Road, Oxford OX1 3RE, UK.
*These authors contributed equally to this work. †Present address: Department of Biochemistry, University of Oxford, South Parks Road, Oxford OX1 3QU, UK. ‡Present address: Department of Biological Sciences, Birkbeck College, Malet Street, London WC1E 7HX, UK. §Present address: Cysal GmbH, Mendelstrasse 11, 48149 Münster, Germany. §Present address: Cysal GmbH, Mendelstrasse 11, 48149 Münster, Germany. ||Present address: Stanford University, School of Medicine, James H. Clark Center, 318 Campus Drive, Stanford, CA 94305–5432, USA. ¶Corresponding author. E-mail: ben.berks@bioch.ox.ac.uk (B.C.B.); susan.lea@path.ox.ac.uk (S.M.L.)

Fig. 1. Spectroscopic analysis of *P. fluorescens* PhoX. (**A**) Changes in the visible spectrum of PhoX (black line) upon addition of 1 mM AMP-PCP (green line). (**B**) EPR spectra of PhoX. The sample was progressively reduced with sodium dithionite as indicated. Alternatively, the sample was treated with Na_2EDTA. (**C**) Changes in the visible spectrum of PhoX (black line) upon addition of 1 mM (light blue line) or 50 mM (dark blue line) Na_2EDTA. The 50 mM Na_2EDTA sample was subsequently buffer-exchanged to remove the EDTA and then supplemented with 100 mM $CaCl_2$ (red line).

high-spin Fe^{3+}. This behavior suggests that PhoX contains a pair of high-spin Fe^{3+} ions rendered EPR-silent by magnetic coupling, with reduction of one of the Fe^{3+} ions to the EPR-silent Fe^{2+} state revealing the EPR signal from the remaining Fe^{3+} ion. Because the two ions in the resulting mixed valence state no longer interact magnetically, it can be inferred that the Fe^{2+} ion has been released from the active-site cofactor. Thus, only the fully oxidized Fe^{3+}-Fe^{3+} state of the PhoX cofactor is catalytically viable. Further addition of sodium dithionite led to reduction of the remaining Fe^{3+} ion, rendering PhoX EPR silent again.

Within the $Fe_AFe_BCa_A$ triangle lies an atom that is within bonding distance of all three metal ions (Fig. 2C and table S3). The close to in-plane geometry suggests that this atom is an oxide ion (O^{2-}). This is confirmed by the structural identity between this part of the PhoX active site and $Fe_2CaO(CCl_3COO)_6(THF)_4$, an inorganic complex containing a μ_3-oxo-bridged $Fe^{3+}Fe^{3+}Ca^{2+}$ cluster with O-donor coordination (11)(fig. S5). The presence of a bridging oxo group explains the strong antiferromagnetic coupling of the two Fe^{3+} ions observed by EPR spectroscopy (Fig. 1B). The intense visible absorption bands of PhoX (Fig. 1A) are, likewise, characteristic of an oxo-bridged dinuclear Fe^{3+} unit (12), although Cys^{179} thiolate-to-Fe_A^{3+} ligand-to-metal charge trans-fer bands are also expected to contribute to the visible spectrum (13). The purple color of PhoX is, thus, distinct in origin from that of the well-known purple acid phosphatases in which the visible absorption is due to a tyrosinate-to-Fe^{3+} charge transfer (14).

PhoX had previously been considered to be an exclusively Ca-dependent enzyme based on the results of metal ion reconstitution experiments [e.g., (7, 8, 15)], although a biosynthetic requirement for Fe in *P. fluorescens* PhoX biosynthesis had been reported (16). In agreement with these earlier reconstitution studies, we found that the enzymatic activity of *P. fluorescens* PhoX was abolished by the metal ion chelator EDTA and that activity could be restored by the addition of Ca^{2+} ions alone (fig. S1C). However, EDTA treatment perturbed, rather than abolished, the visible transitions arising from the Fe_A-Fe_B pair, indicating that the Fe^{3+} ions remain bound to PhoX in the presence of EDTA (Fig. 1C). This conclusion was confirmed by EPR spectroscopy, which showed that only a small proportion (12% by spin quantitation) of the Fe bound to PhoX is extracted by 50-mM EDTA (Fig. 1B). Addition of Ca^{2+} ions to EDTA-treated enzyme restored the visible spectrum (Fig. 1C).

The PhoX-ligand complex structures show that the active-site metal ions form a scaffold that binds the terminal phosphoryl group of the substrate molecule. In the phosphate and vanadate complexes, all five metal ions have bonding interactions with the three terminal oxygen atoms of the ligand (Figs. 2C and 3C and fig. S4, B and C). In these structures, the ligand sits on the $Fe_AFe_BCa_A$ unit, with each terminal oxygen atom of the ligand placed above one of the three metal ions. In the AMP-PCP–bound structure, the phosphate group has a tilted orientation relative to the $Fe_AFe_BCa_A$ plane, and there is no interaction with Ca_A (Fig. 3B). This binding mode permits both the terminal and β-phosphate groups of AMP-PCP to make bonding interactions with Ca_A and Ca_B (Fig. 3B). Modeling studies (not shown) suggest that even for substrates without multiple phosphate groups, an initial tilted binding mode will usually be favored in order to avoid steric clashes with Ca_A and Ca_B. The sole conformational change in the protein that takes place on ligand binding to PhoX is movement of the guanidinium head group of conserved Arg^{385} to form a bonding interaction with one of the terminal oxygen atoms of the ligand (Fig. 2C). Replacing this arginine residue with alanine impairs PhoX activity, suggesting that Arg^{385} contributes to catalysis (table S4).

The primary mechanism of rate enhancement by phosphoryl transfer enzymes is thought to be provision of favorable geometric and electrostatic interactions with the transition state (1, 2).

Fig. 2. Structure of *P. fluorescens* PhoX. (**A**) Cartoon representation of *P. fluorescens* PhoX viewed from above the active site (left) or from the side (right). The blades of the β propeller are shown in different colors and two α subdomains are colored gray. The active-site ions are represented by green (Ca^{2+}), magenta (Fe^{3+}), and cyan (O^{2-}) spheres. (**B**) Clipped surface representation of PhoX with AMP-PCP bound. (**C**) The PhoX active site containing bound phosphate. Interatomic separations that are within bonding distance are shown between the metal ions and protein side chains (gray dashed lines) and between the phosphate ion and coordinating groups (black dashed lines). These distances are tabulated in table S3.
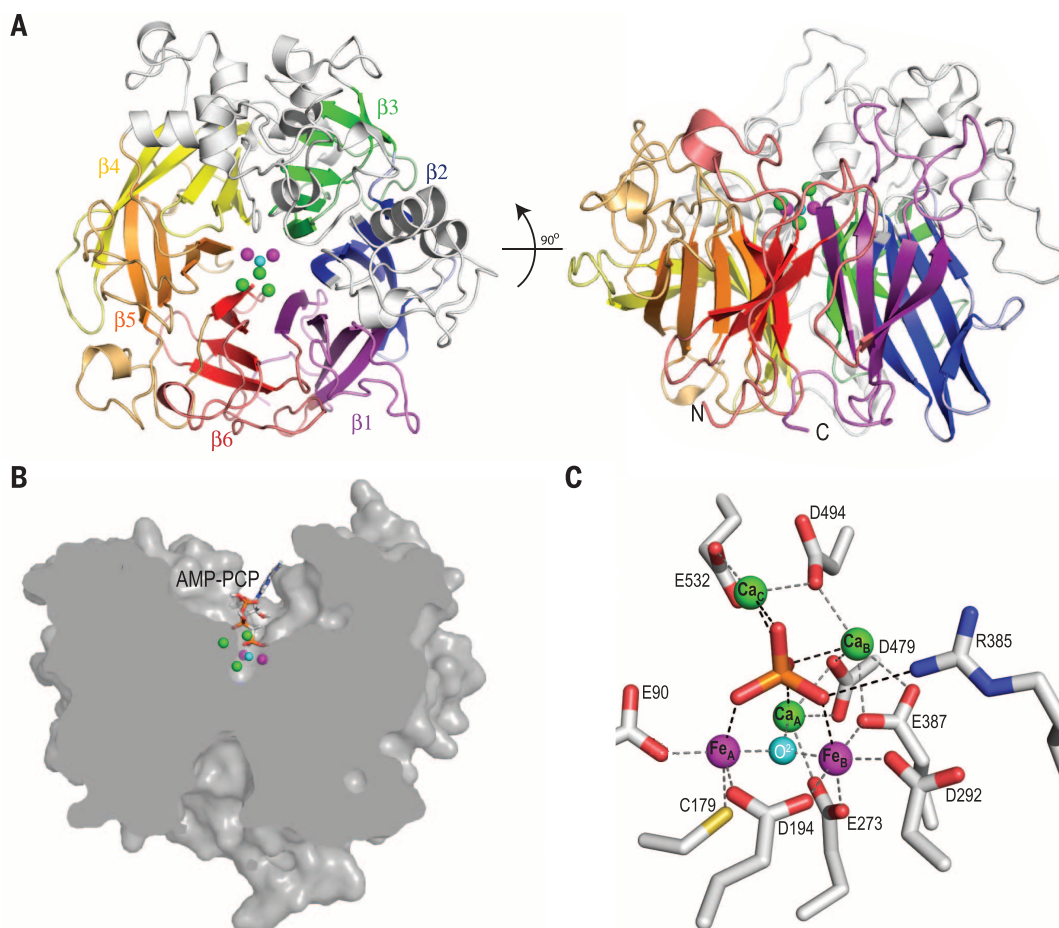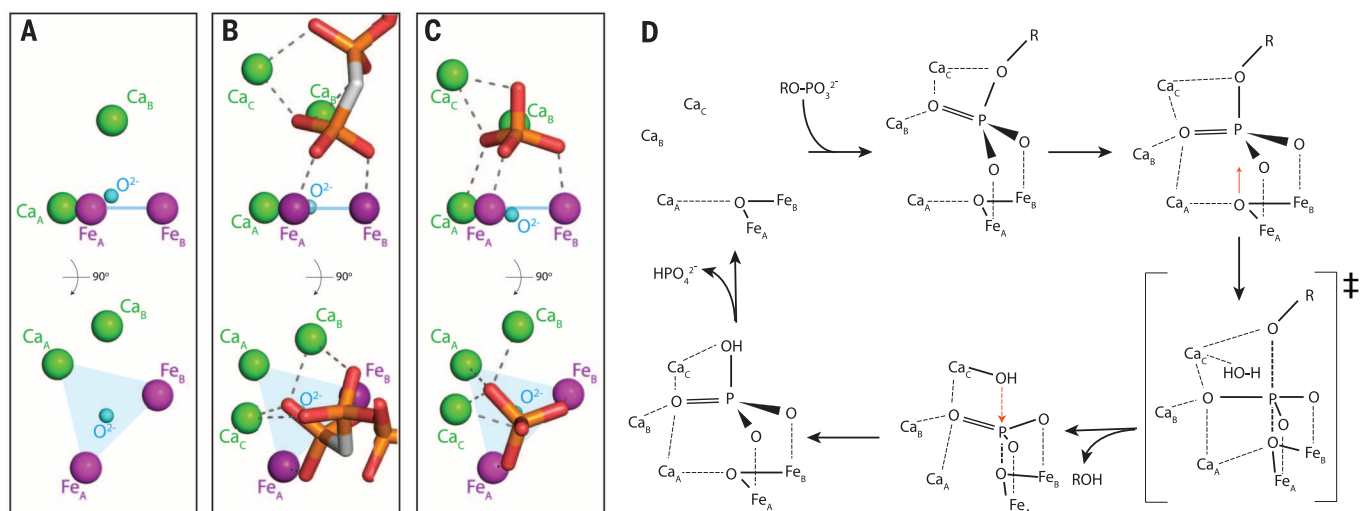
Fig. 3. Ligand binding to the PhoX active-site metals and proposed catalytic cycle. (A to C) The active-site metal ions and exogenous ligands are viewed from the side (top) and from the direction of substrate access (bottom). Atom representation is as in Fig. 2. Dashed lines indicate ion coordination bonds. The plane of the Fe_A-Fe_B-Ca_A ions is shown in blue. Water molecules are omitted for clarity but can be seen in fig. S4, A and D. (A) The native enzyme. Ca_C is not present in this structure. (B) The complex with the nonhydrolyzable substrate analog AMP-CPC. (C) The phosphate complex. (D) Possible model for the mechanism of PhoX. The substrate phosphoryl group initially binds in a tilted orientation (by analogy to the AMP-CPC binding mode), then packs down on to the active site by analogy to the binding mode of phosphate and vanadate. The observed phosphate complex would correspond to the final product complex in this model.

PhoX provides high-valency metal ions that are appropriately positioned to interact with all three terminal oxygen atoms of the phosphoryl group, and in the vanadate complex the ligand is appreciably distorted toward the presumed transition-state geometry (fig. S4C). Leaving group activation through coordination of the oxygen atom of the labile bond by Ca_C may also contribute to catalysis (Fig. 3, C and D, and fig. S4B) (2).

Enzymatic phosphoryl transfer reactions involve in-line displacement of the leaving group by a nucleophile (2). Examination of the PhoX-ligand structures shows that the metal-bridging oxide ion is the only plausible candidate nucleophile (Fig. 3, B and C, and fig. S4, B and C). In the phosphate and vanadate complexes, the oxide ion is positioned below the phosphorus atom and is directly in line with the scissile bond. The oxide ion also blocks access of other potential nucelophiles to the phosphorus atom (in all three PhoX-ligand complexes, the calculated water-accessible surface area of the phosphorus atom trans to the leaving group is 0.0 Å²). There is small-molecule precedent for the hydrolysis of phosphate esters by an oxide ion bridging two Co^{3+} ions (17), and a metal-bridging oxide nucleophile has also been inferred to be present in one purple acid phosphatase (18). Oxide movement toward the phosphoryl P atom during catalysis would be facilitated by the weak Ca_A-oxide interaction and would be consistent with the observed movement of the oxide relative to the $Fe_A$$Fe_B$$Ca_A$ plane in response to ligand binding at the active site (+0.4/−0.2 Å) (Fig. 3, A to C, and fig. S4B). Due to the difficulty in abstracting a μ-bridging oxygen atom from between two Fe^{3+} ions, it is likely that the initial reaction product is resolved by a second in-line nucleophilic at-

tack by a water molecule from the opposite side of the phosphorus atom (Fig. 3D). This water molecule would plausibly be activated by binding to Ca_C because this ion already interacts at the equivalent position with the oxygen atom of the substrate scissile bond (Fig. 3, C and D, and fig. S4B). Nevertheless, we cannot exclude the possibility that the active-site environment labilizes the μ-bridging oxygen atom to allow release of the initial product.

Our structural analysis suggests that PhoX has an almost exclusively inorganic mechanism in which the protein serves as a matrix for the catalytic metal ions. Distinctive features of the PhoX active site include a cofactor that combines Fe and Ca ions, Cys coordination to a Fe^{3+} ion that lacks a redox function, and the use of more than three metal ions to interact with a single phosphoryl group. It is also notable that the $Fe_A$$Fe_B$$Ca_A$O fragment of the cofactor resembles extensively studied synthetic oxide–centered triangular metal complexes (19). Carboxylate-bridged Fe^{3+} pairs are used in other enzymes to catalyze redox reactions with oxygen (12) but in PhoX perform a nonredox role in which the high charge of the iron atoms is exploited to polarize the substrate. Like PhoX, some purple acid phosphatases use a di-iron center to carry out phosphoryl transfer reactions (20). However, in contrast to PhoX, the enzymatically active oxidation state of the iron pair is Fe^{3+}-Fe^{2+} (21), and the catalytic nucleophile is probably a metal-bridging hydroxide ion (20).

Genes coding for PhoX and PhoA are not normally found in the same bacterium (4), suggesting that these two types of alkaline phosphatase have equivalent physiological roles. PhoA activity depends on Zn^{2+} ions, which are present at

low abundance in many environments (22), and this has led to the hypothesis that organisms expressing PhoX have an advantage in P and Zn colimited environments (15). However, our observation that PhoX requires Fe^{3+} ions as cofactors implies that PhoX activity will also be metal-limited by the low bioavailability of Fe in many environments (23). This hypothesis challenges the assumption that P and Fe have biochemically independent effects in colimiting conditions (24) and raises the possibility that combined Zn-Fe-P colimitation may occur in some environments through the requirement for either Zn or Fe for phosphate acquisition from organic phosphates. An environment where such considerations may apply is the western North Atlantic, where inorganic P and Zn concentrations are very low and Fe can also be in short supply (22, 25, 26).

REFERENCES AND NOTES

1. S. C. Kamerlin, P. K. Sharma, R. B. Prasad, A. Warshel, *Q. Rev. Biophys.* **46**, 1–132 (2013).
2. J. K. Lassila, J. G. Zalatan, D. Herschlag, *Annu. Rev. Biochem.* **80**, 669–702 (2011).
3. H. Luo, R. Benner, R. A. Long, J. Hu, *Proc. Natl. Acad. Sci. U.S.A.* **106**, 21219–21223 (2009).
4. M. Sebastian, J. W. Ammerman, *ISME J.* **3**, 563–572 (2009).
5. E. D. Orchard, E. A. Webb, S. T. Dyhrman, *Environ. Microbiol.* **11**, 2400–2411 (2009).
6. M. J. Harke, D. L. Berry, J. W. Ammerman, C. J. Gobler, *Microb. Ecol.* **63**, 188–198 (2012).
7. A. van Mourik, N. M. Bleumink-Pluym, L. van Dijk, J. P. van Putten, M. M. Wösten, *Microbiology* **154**, 584–592 (2008).
8. N. K. Roy, R. K. Ghosh, J. Das, *J. Bacteriol.* **150**, 1033–1039 (1982).
9. J. L. Moseley, C. W. Chang, A. R. Grossman, *Eukaryot. Cell* **5**, 26–44 (2006).
10. Materials and methods are available as supplementary materials on *Science* Online.
11. D. Prodius *et al.*, *Polyhedron* **25**, 2175–2182 (2006).

12. E. I. Solomon *et al.*, *Chem. Rev.* **100**, 235–350 (2000).
13. V. S. Oganesyan, A. J. Thomson, *J. Chem. Phys.* **113**, 5003–5017 (2000).
14. B. P. Gaber, J. P. Sheridan, F. W. Bazer, R. M. Roberts, *J. Biol. Chem.* **254**, 8340–8342 (1979).
15. S. Kathuria, A. C. Martiny, *Environ. Microbiol.* **13**, 74–83 (2011).
16. R. D. Monds, P. D. Newell, J. A. Schwartzman, G. A. O'Toole, *Appl. Environ. Microbiol.* **72**, 1910–1924 (2006).
17. N. H. Williams, A. M. Lebuis, J. Chin, *J. Am. Chem. Soc.* **121**, 3341–3348 (1999).
18. G. Schenk *et al.*, *Proc. Natl. Acad. Sci. U.S.A.* **102**, 273–278 (2005).
19. R. D. Cannon, R. P. White, *Prog. Inorg. Chem.* **36**, 195–298 (1988).
20. N. Mitić *et al.*, *Chem. Rev.* **106**, 3338–3363 (2006).
21. D. L. Wang, R. C. Holz, S. S. David, L. Que Jr., M. T. Stankovich, *Biochemistry* **30**, 8187–8194 (1991).
22. R. W. Jakuba, J. W. Moffett, S. T. Dyhrman, *Global Biogeochem. Cycles* **22**, GB4012 (2008).
23. C. M. Moore *et al.*, *Nat. Geosci.* **6**, 701–710 (2013).
24. M. A. Saito, T. J. Goepfert, J. T. Ritt, *Limnol. Oceanogr.* **53**, 276–290 (2008).
25. J. Wu, W. Sunda, E. A. Boyle, D. M. Karl, *Science* **289**, 759–762 (2000).
26. C. M. Moore *et al.*, *Glob. Change Biol.* **12**, 626–634 (2006).

MARINE MICROBES

Multiple nutrient stresses at intersecting Pacific Ocean biomes detected by protein biomarkers

Mak A. Saito,[1]* Matthew R. McIlvin,[1] Dawn M. Moran,[1] Tyler J. Goepfert,[1] Giacomo R. DiTullio,[2] Anton F. Post,[3] Carl H. Lamborg[1]

Marine primary productivity is strongly influenced by the scarcity of required nutrients, yet our understanding of these nutrient limitations is informed by experimental observations with sparse geographical coverage and methodological limitations. We developed a quantitative proteomic method to directly assess nutrient stress in high-light ecotypes of the abundant cyanobacterium *Prochlorococcus* across a meridional transect in the central Pacific Ocean. Multiple peptide biomarkers detected widespread and overlapping regions of nutritional stress for nitrogen and phosphorus in the North Pacific Subtropical Gyre and iron in the equatorial Pacific. Quantitative protein analyses demonstrated simultaneous stress for these nutrients at biome interfaces. This application of proteomic biomarkers to diagnose ocean metabolism demonstrated *Prochlorococcus* actively and simultaneously deploying multiple biochemical strategies for low-nutrient conditions in the oceans.

Marine photosynthetic activity in the oceans is largely controlled by nutrient and micronutrient availability. Although this process is critical to marine ecosystem structure, ocean-climate interactions, and nutrient cycling processes, the nutrient-addition incubation experiments typically used to assess which nutrients are limiting are time-intensive and subject to artifacts (*1*), making their deployment to broad geographic regions difficult. Nutrient limitation is commonly parameterized in marine ecosystem and biogeochemistry models so that growth is controlled by the single scarcest nutrient (relative to cellular requirements) (*2*); however, multiple scarce nutrients may also influence phytoplankton community structure (*3*, *4*). Molecular methodologies have shown potential for detecting in situ biomarkers for nutrient stress by measurement of up-regulated transcripts or proteins associated with nutrient scarcity (*5*, *6*), but they can have relatively broad biological specificity and can be difficult to deploy to a wide geographic region (*5*). With advances in mass spectrometry, microbial proteins have begun to be directly measured in complex natural environments; recent metaproteomic surveys of oceanic environments have identified and examined the relative abundance of biogeochemically relevant proteins (*7*, *8*).

In this study, we conducted calibrated quantitative mass spectrometry–based protein biomarker measurements using multiple reaction monitoring (MRM) to characterize nutrient limitation patterns for multiple nutrients on the abundant marine cyanobacterium *Prochlorococcus* (*9*). Samples were collected along a ~4500-km meridional transect through the central Pacific and equatorial Pacific Ocean initiating south of the Hawaiian Islands and ending near the Samoan Islands in October of 2011 (Fig. 1A). The equatorial Pacific is an ideal region to examine the range of nutrient stresses affecting phytoplankton be-

cause it crosses several biogeochemical biomes (*10*). Equatorial upwelling caused by Ekman divergence supplies cold, nitrogen-, and phosphorus-rich waters (Fig. 1B and fig. S1) (*11*), resulting in iron limitation of phytoplankton communities (*1*). In contrast, the subtropical gyres to the north and south are highly depleted in multiple nutrients (N, P, and micronutrients; Fig. 1B and fig. S1). The scarcity of multiple nutrients has made it difficult to experimentally determine a single primary limiting nutrient of primary productivity in oligotrophic regions (*3*), and as an alternative, marine ecosystem models have been used to predict iron and nitrogen limitation of the equatorial and subtropical gyre regions of the Pacific, respectively, with a sharp transition between them (*2*, *12*). *Prochlorococcus*, an oxygenic photoautotrophic cyanobacterium, is a major contributor to marine photosynthesis in tropical and subtropical oceanic regions (*1*, *13*) and was observed throughout the transect by its unique divinyl chlorophyll a pigment, particularly in the equatorial upwelling region when total chlorophyll a was also highest (Fig. 1C and fig. S1).

Peptide biomarkers were selected from proteins of interest identified within global metaproteome analyses of the microbial samples taken from this transect. These metaproteome analyses used numerous cyanobacterial genomes and Pacific metagenomes to enable protein identification specific to this region (table S2). Targeted methods were designed using peptide-specific parent to fragment ion transitions (table S3), and synthesized isotope-labeled peptides served as internal standards using MRM on a triple quadrupole mass spectrometer (*14*). Several proteins had been shown in laboratory culture studies of marine cyanobacteria to have potential use as biomarkers of iron and nitrogen stress, including iron deficiency protein IdiA (*5*); flavodoxin, which replaces iron-requiring ferredoxin under iron stress (*15*, *16*); and the global nitrogen response regulator NtcA that serves as a transcriptional activator for alternate forms of nitrogen (such as urea) and is under negative control by ammonium (*17*, *18*). We also targeted the urea transporter of *Prochlorococcus* as an additional nitrogen stress biomarker based on its presence in the metaproteome.

[1]Marine Chemistry and Geochemistry Department, Woods Hole Oceanographic Institution, Woods Hole, MA 02543, USA. [2]College of Charleston, Charleston, SC, USA. [3]Marine Biological Laboratory, Woods Hole, MA 02543, USA.
*Corresponding author. E-mail: msaito@whoi.edu